Toward Elucidating the Physiological Impacts of Residual Stresses in the Colorectum

Y. Zhao[1]
Department of Mechanical Engineering,
University of Connecticut,
Storrs, CT 06269;
Department of Biomedical Engineering,
University of Connecticut,
Storrs, CT 06269

S. Siri
Department of Biomedical Engineering,
University of Connecticut,
Storrs, CT 06269

B. Feng
Department of Biomedical Engineering,
University of Connecticut,
Storrs, CT 06269

D. M. Pierce[2]
Department of Mechanical Engineering,
University of Connecticut,
Storrs, CT 06269;
Department of Biomedical Engineering,
University of Connecticut,
Storrs, CT 06269
e-mail: dmpierce@engr.uconn.edu

Irritable bowel syndrome afflicts 10–20% of the global population, causing visceral pain with increased sensitivity to colorectal distension and normal bowel movements. Understanding and predicting these biomechanics will further advance our understanding of visceral pain and complement the existing literature on visceral neurophysiology. We recently performed a series of experiments at three longitudinal segments (colonic, intermediate, and rectal) of the distal 30 mm of colorectums of mice. We also established and fitted constitutive models addressing mechanical heterogeneity in both the through-thickness and longitudinal directions of the colorectum. Afferent nerve endings, strategically located within the submucosa, are likely nociceptors that detect concentrations of mechanical stresses to evoke the perception of pain from the viscera. In this study, we aim to: (1) establish and validate a method for incorporating residual stresses into models of colorectums, (2) predict the effects of residual stresses on the intratissue mechanics within the colorectum, and (3) establish intratissue distributions of stretches and stresses within the colorectum in vivo. To these ends we developed two-layered, composite finite element models of the colorectum based on our experimental evidence and validated our approaches against independent experimental data. We included layer- and segment-specific residual stretches/stresses in our simulations via the prestrain algorithm built into the finite element software FEBIO. *Our models and modeling approaches allow researchers to predict both organ and intratissue biomechanics of the colorectum and may facilitate better understanding of the underlying mechanical mechanisms of visceral pain.* [DOI: 10.1115/1.4051846]

Keywords: colorectum, residual stresses, residual stretches, opening-angle experiments, finite element modeling, mechanobiology

1 Introduction

The biomechanics of visceral organs govern the macroscopic mechanical organ stimuli and the local mechanical stresses and strains at sensory nerve endings [1,2]. Understanding and predicting these biomechanics will further advance our understanding of visceral pain and complement the existing literature on visceral neurophysiology [3–5]. Visceral pain is a leading complaint from patients with irritable bowel syndrome, a condition afflicting 10–20% of the world's population [6,7]. Conscious perception from the viscera usually present as discomfort and/or pain, which is not evoked reliably by noxious stimuli like heating, cutting, pinching, or piercing, but caused by mechanical distension of hollow visceral organs like the distal colon and rectum (colorectum) [3,8]. Clinically, patients with irritable bowel syndrome show increased sensitivity to colorectal distension and heightened perceptions of pain during normal mechanical bowel movements [8–10]. Consistent with the mechanical stimuli which evoke visceral pain, the vast majority (70–80%) of sensory afferent nerve endings that innervate the colorectum are mechanosensitive [3]. Thus, visceral pain has a unique biomechanical component.

Mechanosensitive afferents undertake neural encoding of mechanical stimuli in the colorectum, and most of these afferents have unmyelinated C-type axons with free nerve endings embedded within the colorectum [3]. Afferent endings exist in all sublayers of the colorectum except in the serosa [11,12], i.e., the mucosal, submucosal, circular muscular, myenteric plexus, and longitudinal muscular layers. The colorectum is thus heterogenous through the thickness, as recently characterized by us using both biaxial extension tests on layer-separated tissue patches [13,14] and nonlinear imaging via second harmonic generation [15]. These combined data reveal that the submucosal layer, containing dense collagen, is the primary load-bearing structure of the colorectum, along with the two muscular layers [14]. Interestingly, the submucosa and myenteric plexus (sandwiched by the two muscular layers) also present significantly higher densities of afferent nerve endings [12]. We contend that these regions within the colorectum contain both concentrated loads and high densities of afferent nerves not by mere coincidence, but that colorectal mechanotransduction and mechanonociception takes place by afferents strategically located in the submucosa and myenteric plexus. Thus, local mechanical stresses in focal regions of the colorectum could have profound impact on the mechanotransduction that underlies perception of visceral pain.

The local, intratissue mechanical stresses result not only from the mechanical properties of different sublayers of the colorectum but are also significantly affected by residual stresses widely present in healthy soft tissues under physiological conditions, e.g., the arterial walls [16–18]). Indeed, the existence of residual stresses in healthy arteries is long and well established [19–23]. Residual stresses tend to homogenize the stress distribution through the thickness of arteries in vivo [24–31]. Yet, no analogous understanding exists for the colorectum.

In separating the layers of the colorectum, we observed that square specimens changed their circumferential lengths from the

[1]Present address: School of Aerospace Engineering and Applied Mechanics, Tongji University, Shanghai 200092, China.
[2]Corresponding author.
Manuscript received April 10, 2021; final manuscript received July 12, 2021; published online September 1, 2021. Assoc. Editor: Raffaella De Vita.

Table 1 The outer and inner radii of composite colorectums, and the wall-thickness of the inner composite (mucosa and submucosa), from the colonic, intermediate, and rectal segments of colorectums of mice under a constant internal pressure of 10 mmHg (M±SD), where *n* is the number of samples

Segment	Outer radius (mm)	Inner radius (mm)	Inner thickness (mm)
Colonic ($n=6$)	1.80 ± 0.167	1.68 ± 0.191	0.0872 ± 0.029
Intermediate ($n=6$)	1.80 ± 0.297	1.65 ± 0.199	0.107 ± 0.026
Rectal ($n=6$)	1.80 ± 0.460	1.62 ± 0.219	0.113 ± 0.020

complete composite configuration to the layer-separated configuration. We quantified these dimensional changes and our results indicated compressive and tensile circumferential residual stresses within the inner and outer composite layers, respectively, and with increasing magnitudes from the colonic to rectal segments. We further quantified the segment-specific residual stretches/stresses by completing opening-angle tests. We made longitudinal cuts in intact rings of colorectums from the colonic, intermediate, and rectal segments and quantified the resulting angles using optical methods [13]. However, we still don't know how residual stresses alter the total intratissue mechanical stresses within different regions of the colorectum, and thus, the biomechanical and mechanobiological roles of residual stresses on the intratissue mechanics of the colorectum remain unclear.

To better understand the underlying mechanisms of visceral pain by mechanotransduction in the colorectum, and establish potential treatment targets, we seek to predict local organ/tissue biomechanics, particularly mechanical stresses, from bulk mechanical colorectal distension and peristalsis by systematically incorporating residual stresses. To this end, in this study we aim to: (1) establish and validate a method for incorporating residual stresses in models of colorectums, and (2) predict the effects of residual stresses on the intratissue distributions of stretches and stresses within the colorectum, and (3) establish through-thickness and longitudinal, intratissue distributions of stretches and stresses within the colorectum under conditions mimicking those in vivo. To these ends, we developed two-layered, composite finite element (FE) models of the colorectum based on our experimental evidence and validated our approach against independent experimental data. We incorporated residual stretches/stresses within the individual layers of our FE simulations the colorectum using the prestrain algorithm in FEBIO. The results of our FE simulations indicate that these residual stretches/stresses have a profound impact on the local (intratissue) mechanics, particularly through the thickness of the colorectum.

2 Materials and Methods

2.1 Experimental Evidence. We previously completed pressure-diameter tests on the intact (complete composite) distal 30 mm of colorectums of mice (i.e., within the colonic, intermediate, and rectal segments) [14,32]. In completing these mechanical tests, we quantified the cylindrical geometry of the colorectums in the near-stress-free configurations (assumed as reference configurations) under a constant internal pressure of 10 mmHg [33], reported as mean±standard deviation (M±SD) in Table 1.

We previously also completed biaxial extension tests on the distal 30 mm of colorectums of mice (again the colonic, intermediate, and rectal segments) dissected into inner (mucosa and submucosa) and outer (muscular layers and serosa) composite layers [14]. In preparing the layer-separated specimens of colorectum, we observed that square specimens changed their circumferential lengths from the complete composite configuration ($7\times7\,\text{mm}^2$) to the layer-separated configuration, reported as M±SD in Table 2. The corresponding radial lengths of the layer-separated inner and outer composite specimens did not change length appreciably after dissection.

We also quantified the opening angles from the intact (complete composite) distal 30 mm of colorectums of mice (again the colonic, intermediate, and rectal segments) [13]. We cut open rings of composite colorectums 2 mm in length longitudinally (in the radial-axial plane) to form arcs and directly measured the subtended angles through the inner midpoint of the arcs, reported as M±SD in Table 3 [13].

2.2 Constitutive model for the Composite Colorectum. We recently established and validated a constitutive model for mouse colorectum capturing longitudinal and through-thickness biomechanical heterogeneity [32]. Briefly, we used a multiplicative split of the strain-energy function Ψ into volumetric and isochoric contributions as $\Psi = U(J) + \bar{\Psi}$, where $U(J) = \kappa(J-1)^2/2$, $J = \det\mathbf{F}$ (the Jacobian of the deformation gradient), and κ is a non-physical, positive penalty parameter used to enforce near incompressibility. We also used the multiplicative decomposition $\bar{\mathbf{F}} = J^{-1/3}\mathbf{F}$, and similarly the isochoric right Cauchy-Green tensor $\bar{\mathbf{C}} = J^{-2/3}\mathbf{C}$, where $\mathbf{C} = \mathbf{F}^{\mathrm{T}}\mathbf{F}$. We modeled the individual mechanical responses of the inner and outer composites using an additive decomposition $\bar{\Psi} = \bar{\Psi}_{\mathrm{IM}} + \bar{\Psi}_{\mathrm{FN}}$, with an isotropic (neo-Hookean) matrix $\bar{\Psi}_{\mathrm{IM}}(\bar{I}_1) = \mu(\bar{I}_1 - 3)/2$, where $\mu > 0$ is the shear modulus of the underlying matrix in the reference configuration, $\bar{I}_1 = \mathrm{tr}\bar{\mathbf{C}}$ is the first invariant of $\bar{\mathbf{C}}$, and with a contribution from a network of fibers [34,35]

$$\bar{\Psi}_{\mathrm{FN}} = \int_{\Omega} \rho(\mathbf{M}) \frac{k_1}{2k_2} \left(\exp\left[k_2 (\bar{I}_4 - 1)^2 \right] - 1 \right) \mathcal{H}(\bar{I}_4 - 1)\, \mathrm{d}\Omega \quad (1)$$

where $k_1 > 0$ is a stress-like material parameter, $k_2 > 0$ is a dimensionless parameter, $\bar{I}_4 = \mathbf{M}\cdot\bar{\mathbf{C}}\mathbf{M}$ is the isochoric fourth pseudo-invariant of $\mathbf{M}$ (the reference angular orientation of a single fiber), and $\mathcal{H}$ is a Heaviside function evaluated at $(\bar{I}_4 - 1)$, i.e., the collagen fibers only support tension. Here, $\rho(\mathbf{M})$ is an orientation distribution function characterizing the local angular density of the fiber network as [35]

$$\rho(\mathbf{M}, \mathbf{D}) = \frac{\sin\theta}{|\mathbf{D}|^{1/2}(\mathbf{M}^{\mathrm{T}}\mathbf{D}^{-1}\mathbf{M})^{3/2}} \quad (2)$$

where $\mathbf{D}$ is a second-order, symmetric, positive-definite tensor defined in spherical coordinates, $\sin\theta$ accounts for the change from Cartesian to spherical variables, and with $1/4\int_{\Omega}\rho(\mathbf{M})\,\mathrm{d}\Omega = 1$, where $\Omega = \mathbf{M} \in \mathbb{R}^3 : |\mathbf{M}| = 1$ is the unit sphere.

Table 2 The circumferential length of layer-separated inner (mucosa and submucosa) and outer (muscular layers and serosa) composites after dissection from initial, complete composite specimens of $7\times7\,\text{mm}^2$ from the colonic, intermediate, and rectal segments of colorectums of mice (M±SD), where *n* is the number of samples [32]

Segment	Inner Composite (mm)	Outer Composite (mm)
Colonic ($n=10$)	7.12 ± 0.028	6.83 ± 0.051
Intermediate ($n=11$)	7.15 ± 0.025	6.79 ± 0.054
Rectal ($n=11$)	7.14 ± 0.029	6.68 ± 0.049

Table 3 The opening angles of complete composite specimens taken from the colonic, intermediate, and rectal segments of colorectums of mice (M±SD), where *n* is the number of samples[13]

Segment	Opening Angle (deg)
Colonic ($n=7$)	42.4 ± 12.8
Intermediate ($n=7$)	58.4 ± 11.8
Rectal ($n=7$)	119.4 ± 17.8

Table 4 Prescribed values of prestretch ($\lambda_{p,\theta}$) for the inner and outer composite layers for each segment (i.e., within the colonic, intermediate, and rectal segments)

Segment	Inner composite	Outer composite
Colonic	0.983	1.025
Intermediate	0.979	1.031
Rectal	0.981	1.047

To model the through-thickness biomechanical heterogeneity at the colonic, intermediate, and rectal segments of the colorectum we leveraged the model parameters (μ, k_1, k_2, α), we previously established for the inner (mucosa and submucosa) and outer (muscular layers and serosa) composite layers [32].

2.3 Finite Element Simulations Including Residual Stretches/Stresses. We established FE models for predicting (a) the opening-angle test of the composite colorectum ring (for validation) and (b) the pressure-diameter test of the composite colorectum under applied intraluminal pressure (to determine the intratissue distributions of stretch and stress in vivo with and without considering residual stretches/stresses). To create our FE models, we specified the reference configurations (inner and outer diameters and layer thicknesses) using data in Table 1, see Fig. 1.

We incorporated the distribution of residual stretches/stresses using data in Table 2 and implemented these via the prestrain algorithm build into FEBIO (R2.8.5, University of Utah, UT) [36,37]. Specifically, we assumed that the stretches were homogeneous in each element and defined the prestretch by imposing a deformation gradient tensor

$$\mathbf{F}_{\mathrm{p}} = \begin{bmatrix} \lambda_{p,r} & 0 & 0 \\ 0 & \lambda_{p,\theta} & 0 \\ 0 & 0 & \lambda_{p,z} \end{bmatrix} \tag{3}$$

presented in cylindrical coordinates (r, θ, z), where $\lambda_{p,r}$, $\lambda_{p,\theta}$, and $\lambda_{p,z}$ are layer-specific, prescribed prestretches. We prescribed $\lambda_{p,\theta}$ for the inner and outer composites as given in Table 4, while the remaining prestretches $\lambda_{p,r} = \lambda_{p,z} = 1$.

We completed all simulations using FEBIO [36].

2.4 Validation: The Opening-Angle Test. To predict the opening angles at the colonic, intermediate, and rectal segments, we exploited the symmetry of the boundary value problem. We

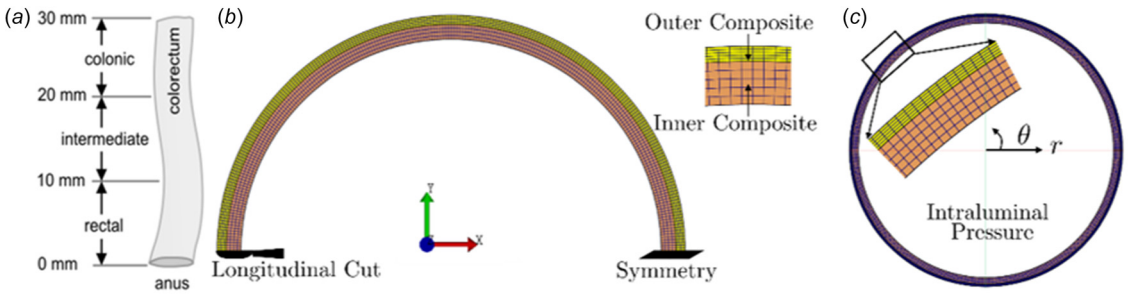

Fig. 1 Modeling the colorectum: (*a*) schematic illustrating the longitudinal segments of the colorectum; (*b*) finite element (FE) model used for predicting the opening-angle test of the composite colorectum ring (for validation); and (*c*) FE model used for predicting the pressure-diameter test of the composite colorectum under applied intraluminal pressure (to determine the intratissue distributions of stretch and stress in vivo with and without considering residual stretches/stresses)

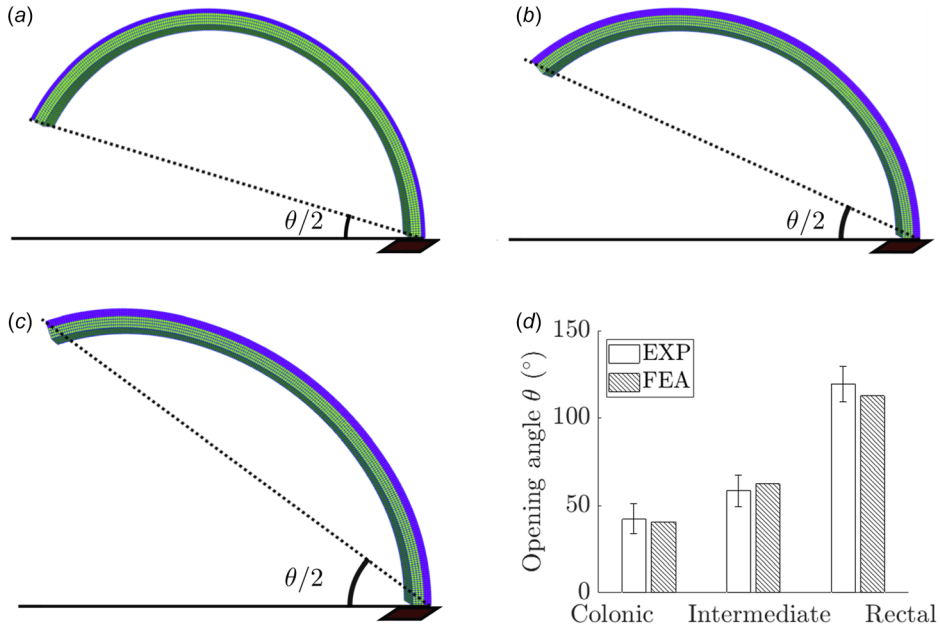

Fig. 2 Predictions of the opening angles θ for different colorectum segments: (*a*) colonic, (*b*) intermediate, and (*c*) rectal. (*d*) Direct comparison of the predicted opening angles (finite element analyses) versus the experimental measurements presented as M±SD [13].

modeled only half model of the composite (intact) colorectum as two-layered, residually stressed cylinder which we meshed using 1200 tri-linear hexahedral elements for each of the two layers. To release the residual stresses, we modeled a longitudinal cut (see Fig. 1(*a*)) along the length of the colorectum, wherein nodes on the cut surface had no constraints on their displacement degrees-of-freedom. We enforced a fixed boundary condition on remaining symmetry face (without the longitudinal cut), and we directly measured the opening angle from the simulations at equilibrium.

2.5 Predictions: The Pressure-Diameter Test. To predict the intratissue stretches/stresses at the colonic, intermediate, and rectal segments during the pressure-diameter test we modeled the composite (intacted) colorectums as two-layered, tubular segments both with and without accounting for residual stretches/stresses. Exploiting plane-strain conditions, we modeled only a 2 mm longitudinal segments of intact colorectums meshed using 2400 tri-linear hexahedral elements for each of the two layers. We applied symmetry boundary conditions on both faces of the model normal to the longitudinal direction, fixed two radial rows of nodes normal to the radial direction (to prevent rigid-body rotations), and stretched the model axially by 30%, consistent with the experimentally determined axial elongation of the colorectum undergoing intraluminal distension with 60 mmHg internal pressure. We then increased the intraluminal pressure linearly from 0 to 100 mmHg. To assess the effects of residual stretches/stresses on the intratissue stretches/stresses within the colorectum under intraluminal pressure, we performed three related simulations: (1) zero intraluminal pressure including residual stresses, (2) 100 mmHg intraluminal pressure without including residual stresses, and (3) 100 mmHg intraluminal pressure including residual stresses.

3 Results

3.1 Validation: The Opening-Angle Test. We successfully simulated the process of releasing the principal (circumferential) residual stresses at the colonic, intermediate, and rectal segments by creating a longitudinal cut, see Figs. 2(*a*)–2(*c*), respectively.

Our predictions (with finite element analyses) of the opening angles within the colonic, intermediate, and rectal segments (40.6 deg, 62.8 deg, and 112.7 deg, respectively) compare favorably with the experimental measurements from Ref. [14], see Fig. 2(*d*).

3.2 Predictions: The Pressure-Diameter Test. We successfully simulated the pressure-diameter test with the intraluminal pressure increasing linearly from 0 to 100 mmHg at (1) zero intraluminal pressure including residual stresses, (2) 100 mmHg intraluminal pressure without including residual stresses, (3) 100 mmHg intraluminal pressure including residual stresses. To compare the results qualitatively, we first plotted the distributions in circumferential stresses for each segment (colonic,

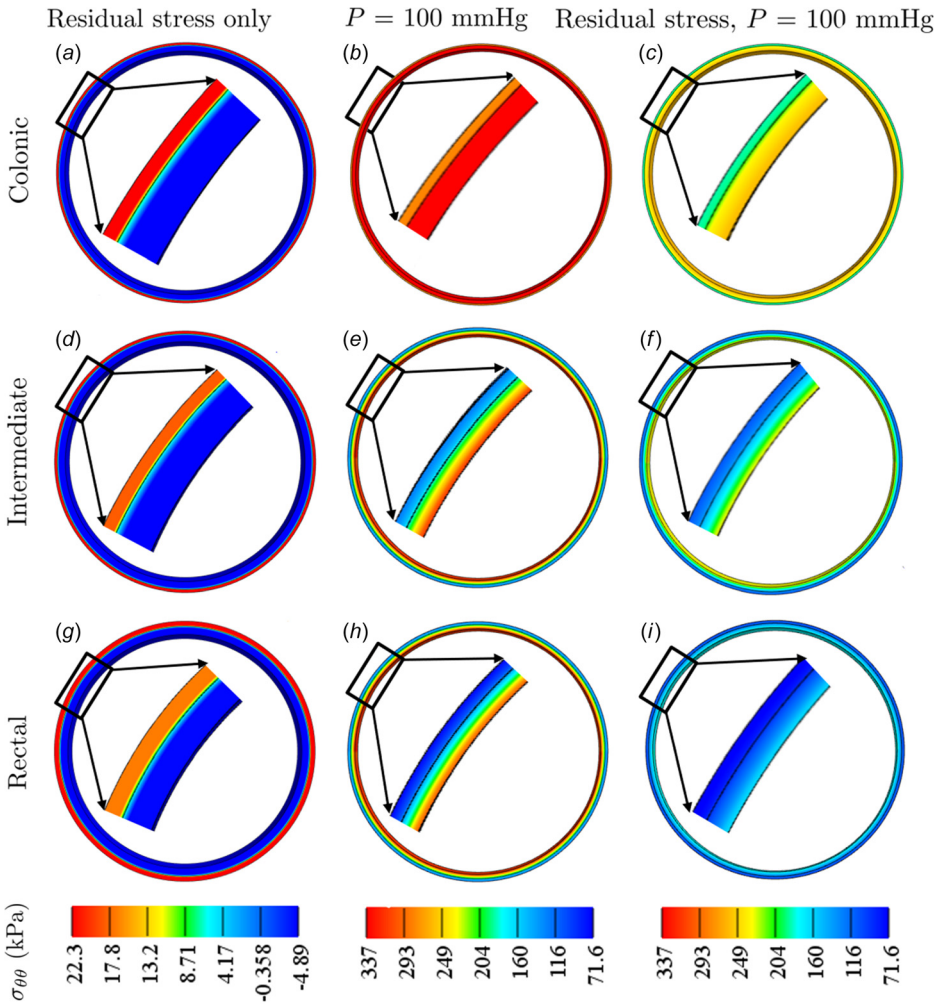

Fig. 3 Distributions of circumferential stressed for (*a*)–(*c*) colonic, (*d*)–(*f*) intermediate, and (*g*)–(*h*) intermediate segments of the colorectum predicted from simulations (*a*), (*d*), and (*g*) including residual stresses only, (*c*), (*e*), and (*h*) at $P = 100$ mmHg without including residual stresses, and (*d*), (*f*), (*i*) at $P = 100$ mmHg including residual stresses

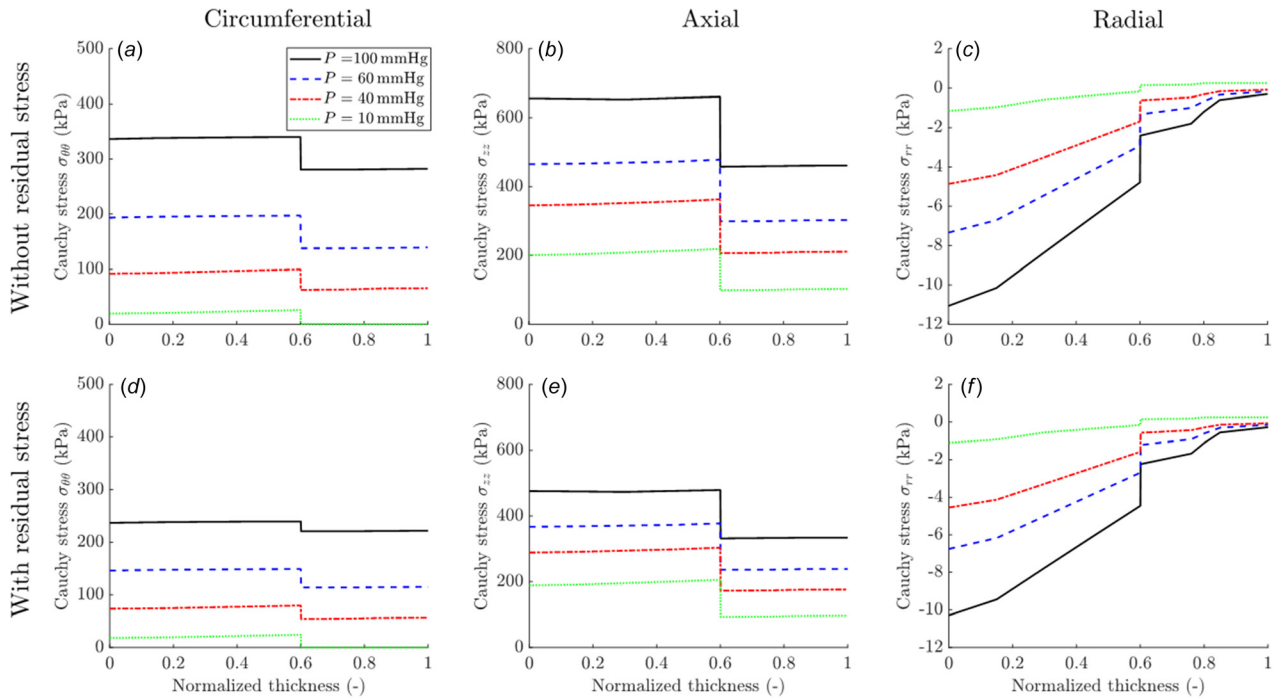

Fig. 4 Plots of the (*a*) and (*d*) circumferential, (*b*) and (*e*) axial, and (*c*) and (*f*) radial (principal) Cauchy stresses through the normalized thickness of the colonic segment of the colorectum at $P = 10, 40, 60, 100$ mmHg both (*a–c*) without and (*d–f*) with considering residual stresses

intermediate, rectal) in the three conditions detailed above, see Fig. 3. Specifically, Figs. 3(*a*), 3(*d*), and 3(*g*), 3(*c*), 3(*e*), and 3(*h*), and 3(*d*), 3(*f*), and 3(*i*) show the simulation results considering (1) only residual stresses, (2) no residual stresses at $P = 100$ mmHg, and (3) the two effects combined, respectively.

To compare the results quantitatively, we plotted the (principal) Cauchy stresses ($\sigma_{\theta\theta}$, σ_{zz}, and σ_{rr}) through the normalized thickness (in the radial direction) for the colonic (Fig. 4), intermediate (Fig. 5), and rectal (Fig. 6) segments of the colorectum.

We also plotted (principal) Green–Lagrange strains ($E_{\theta\theta}$, E_{zz}, and E_{rr}) through the normalized thickness (in the radial direction) for the colonic (Fig. 7), intermediate (Fig. 8), and rectal (Fig. 9) segments of the colorectum.

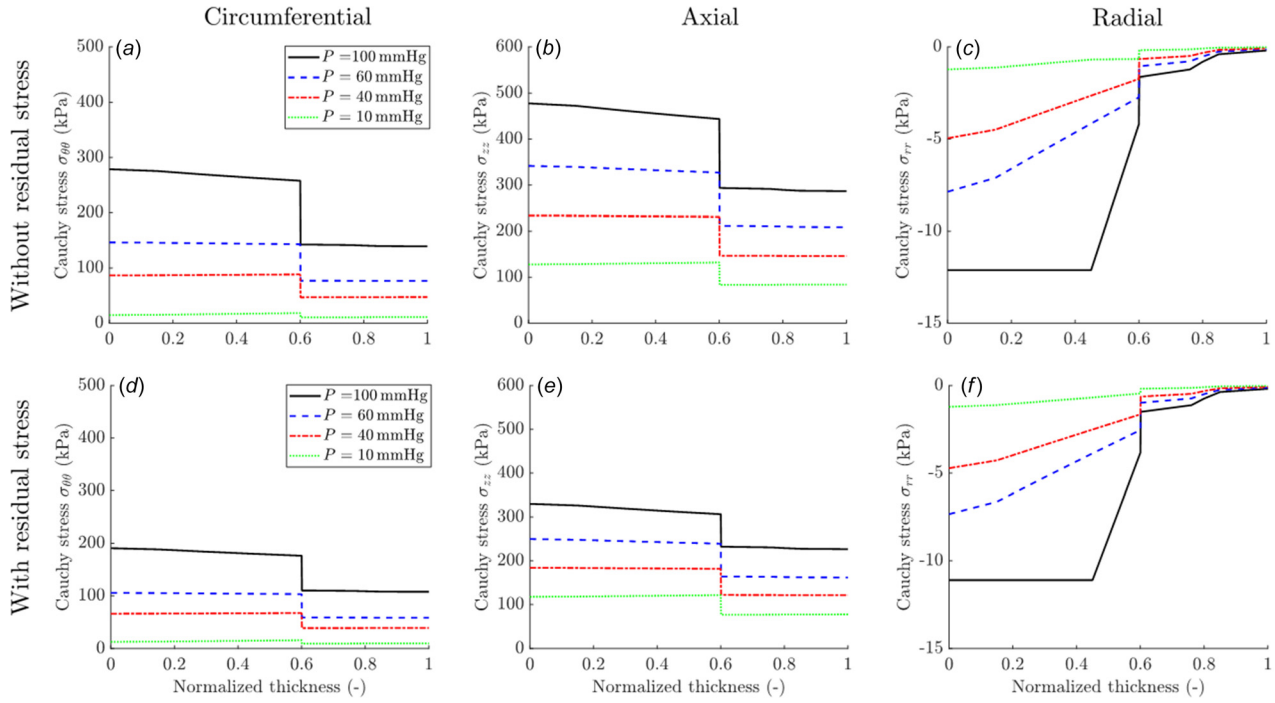

Fig. 5 Plots of the (*a*) and (*d*) circumferential, (*b*) and (*e*) axial, and (*c*) and (*f*) radial (principal) Cauchy stresses through the normalized thickness of the intermediate segment of the colorectum at $P = 10, 40, 60, 100$ mmHg both (*a–c*) without and (*d–f*) with considering residual stresses

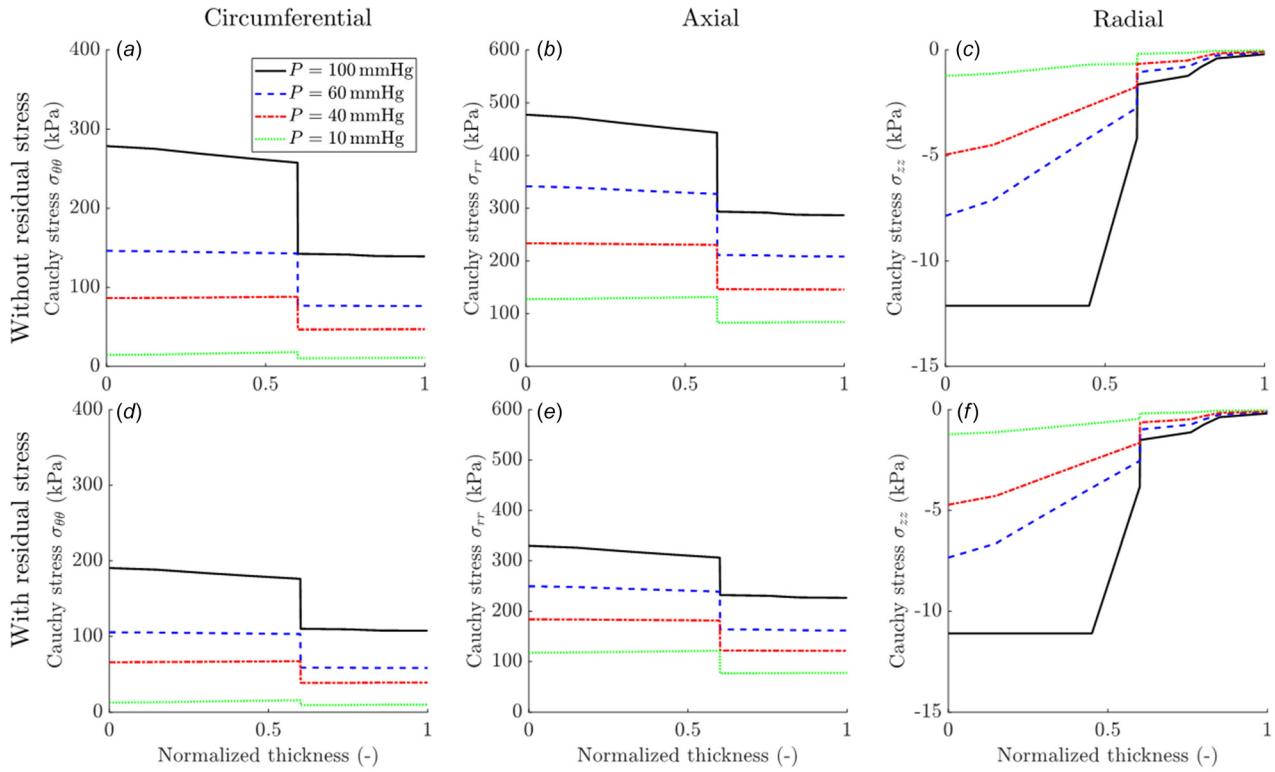

Fig. 6 Plots of the (*a*) and (*d*) circumferential, (*b*) and (*e*) axial, and (*c*) and (*f*) radial (principal) Cauchy stresses through the normalized thickness of the rectal segment of the colorectum at $P = 10, 40, 60, 100$ mmHg both (*a–c*) without and (*d–f*) with considering residual stresses

4 Discussion

We focused this study on predicting residual stresses within colorectums and quantifying the macro- and microscale intratissue mechanics of the colorectum. We modeled the colorectum as a two-layered, residually stressed composite. We included residual stresses in our models as a form of prestretch calibrated from our experimental measurements of separated layers of tissue. As validation of our approach, we successfully predicted the

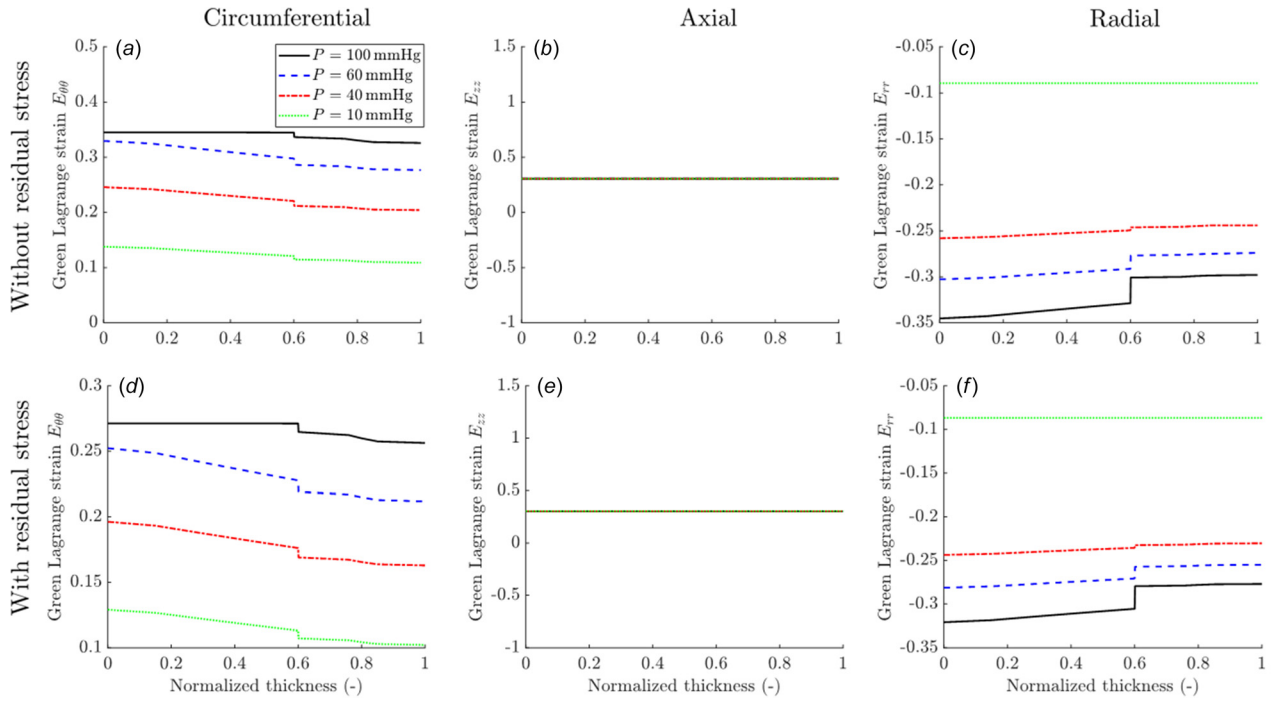

Fig. 7 Plots of the (*a*) and (*d*) circumferential, (*b*) and (*e*) axial, and (*c*) and (*f*) radial (principal) Green–Lagrange strains through the normalized thickness of the colonic segment of the colorectum at $P = 10, 40, 60, 100$ mmHg both (*a–c*) without and (*d–f*) with considering residual stresses

(independent) experimentally determined opening angles. With confidence in our models, we quantified the distributions intratissue stretches/stresses in the colorectal wall during intraluminal distension with and without considering residual stresses. These intratissue mechanical conditions may provide insight both to structure-function relationships and to mechanobiology within the colorectum.

4.1 Validation: The Opening-Angle Test. Independently and accurately predicting independent experimental measurements of the opening angle test validates our method to include residual stresses within our models of the colorectum, cf. Fig. 2. Separating the layers of intact (composite) specimens of tissue leads to significant circumferential elongation of the inner composite and corresponding circumferential shrinkage of the outer composite, cf. Table 1. These deformations relieve residual stresses and indicate that the inner and outer composites are physiologically in compression and tension, respectively. For tubular composite (Fig. 2(*a*)), the longitudinal cut releases the residual stresses and produces deformed configuration with opening angles (θ). In Fig. 2, our simulated results of θ agree well with the mean experimental values and fall well within one standard deviation from the mean. Moving proximal to distal along the colorectum (colonic to rectal segments), the colorectum presents increased opening angles, consistent with the measured residual stretches in Table 1, and thus, the internal residual stretches/stresses increase along the length.

4.2 Predictions: The Pressure-Diameter Test. Prior to reviewing the intratissue distributions of stresses and stretches, both qualitatively and quantitatively, we note that an intracolonic pressure of zero mmHg is innocuous, whereas 60 mmHg is in the noxious pressure range for mice [38]. An intracolonic pressure of 100 mmHg recapitulates the magnitude of focal mechanical stresses in experimental studies of punctate probing of colorectal wall with a von Frey-like nylon filament [39]. In the cylindrical colorectum (modeled as a two-layered, residually stressed composite) undergoing internal pressurization, the cylindrical basis is coincident with the principal basis, such that $\sigma_1 = \sigma_{\theta\theta}$, $\sigma_2 = \sigma_{zz}$, and $\sigma_3 = \sigma_{rr}$.

Starting from our qualitative results, Figs. 3(*a*), 3(*d*), and 3(*g*) shows that with only the initial distributions of residual stresses, compressive circumferential stresses appear within the softer inner composite, which may trigger mechanical instabilities with buckling [40,41]. Figures 3(*b*), 3(*e*), and 3(*h*) shows that, in response to pure intraluminal pressure at 100 mmHg, tensile circumferential stresses appear in both the inner and outer composite layers, and the maximum stresses present at the inner radius (submucosal space) with values decreasing toward the outermost radius, where we observed the lowest circumferential stresses.

Finally, Figs. 3(*c*), 3(*f*), and 3(*i*) shows that the residual stretches smooth the distribution of circumferential stresses in the radial direction of the colorectum tissue The heterogeneity of the colorectal wall generates the discontinuity in the circumferential stresses at the interface of the composite layers.

Quantitatively, plots of the distributions of principal stresses (Figs. 4–6) and strains (Figs. 7–9) through the wall thickness of the pressurized colorectum highlight the physiological impact of residual stresses. Overall, under applied internal pressure, we found the composite in tension in the circumferential and axial directions through the thickness, while there was compression in the radial direction. Furthermore, the magnitude of radial stresses (σ_{rr}) was much smaller than that of circumferential and axial stresses in the cases both with and without residual stresses. The stress components $\sigma_{\theta\theta}$, σ_{zz}, and σ_{rr} are all discontinuous at the interface of the inner and outer composite layers. We found that higher internal pressures resulted in larger discontinuities in the stresses, and that residual stresses decreased both the overall magnitude of the stresses and also the interface discontinuity, particularly under noxious internal pressures. Our findings in the colorectum are consistent with prior analyses of arteries where residual stresses create a more uniform distribution of stresses in the homeostatic state [27,42].

We observed the maximum circumferential stresses occurred at the inner radius of the cylindrical composite, and affected by the

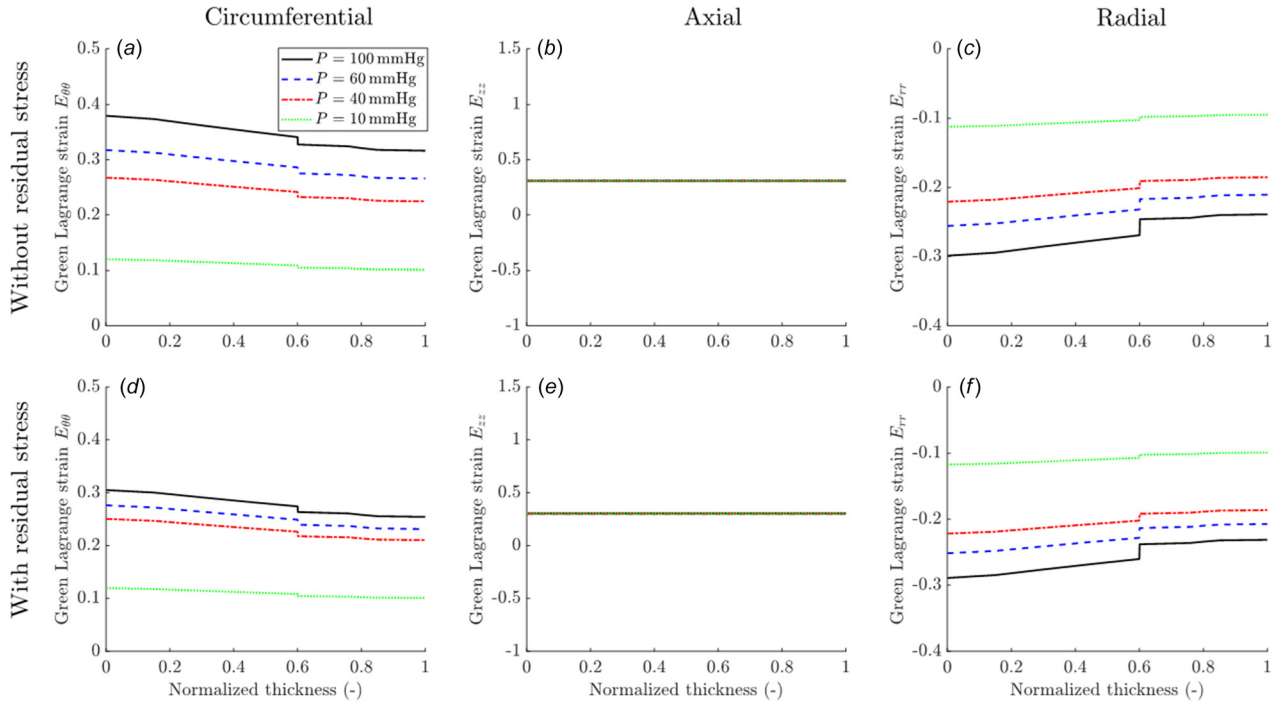

Fig. 8 Plots of the (*a*) and (*d*) circumferential, (*b*) and (*e*) axial, and (*c*) and (*f*) radial (principal) Green–Lagrange strains through the normalized thickness of the intermediate segment of the colorectum at $P = 10, 40, 60, 100$ mmHg both (*a–c*) without and (*d–f*) with considering residual stresses

residual stresses, the maximum circumferential stresses at $P = 100$ mmHg reduced from 337 kPa, 278 kPa, and 269 kPa (without residual stresses) to 236 kPa, 190 kPa, and 142 kPa (with residual stresses) in the colonic, intermediate, and rectal segments, respectively. Similarly, affected by residual stresses, the maximum magnitude of axial stresses (in the inner layer composite) at $P = 100$ mmHg decreased from 656 kPa, 477 kPa, and 470 kPa (without residual stresses) to 475 kPa, 330 kPa, and 278 kPa (with residual stresses) in the colonic, intermediate, and rectal segments, respectively. Simultaneously, the principal strains (Figs. 7–9) demonstrated similar distributions through the wall thickness and were similarly impacted by including residual stresses, except for the axial strain which we fixed at 0.3 (boundary condition) to mimic the experiment (we designed the experiment itself to mimic the conditions in vivo). Note that the stresses $\sigma_{\theta\theta}$ and σ_{zz} show comparable magnitudes when $E_{\theta\theta} \approx 0.3$ ($P \approx 60$ mmHg) and $E_{zz} \approx 0.3$ ($P \approx 10$ mmHg), which is consistent with our observations experimentally.

Our simulations indicated that the most important (physiologically relevant) influence of the residual stresses is the reduction in magnitudes of the maximum circumferential and axial stresses. Residual stretches, for example, in the rectal segment lead to reductions of 47.2% and 41.7% in $\sigma_{\theta\theta}$ and σ_{zz}, respectively. Additionally, we found that larger residual stretches resulted in more pronounced reductions in stresses, cf. Ref. [27].

Our results highlight the importance of modeling colorectum as a residually stressed, multilayered composite where differences in the mechanical properties of the layers lead to discontinuous stress/strain patterns through the wall thickness. Physiologically, the predicted distributions of circumferential stresses within the colorectum strongly indicates that the inner (mucosal and submucosal) layer is the main load bearing structure of the colorectum, consistent with our previous experimental observations [13,14]. Residual stresses within the inner and outer composite layers play a critical role in the physiological, biomechanical performance of the colorectum. Due to the highly nonlinear behavior of the colonic tissue [13,14,32], our results indicate the importance of including residual stretches/stresses in analyses of macro- and microscale intratissue mechanics of the colorectum. Accurate predictions of intratissue mechanical state become especially important when analyzing visceral pain evoked by mechanical stimuli, where thresholds above a homeostatic stress or strain may trigger a response.

Our results indicate the importance of including residual stretches/stresses in analyses of macro- and microscale intratissue mechanics of the colorectum. Sensory nerve endings embedded in the colorectal wall undertake visceral mechanotransduction and nociception, which encode intratissue mechanical stresses and stretches into trains of action potentials to inform the central nervous system. Our recent anatomic study on optically cleared colorectum indicates concentrated sensory nerve endings in the submucosa [12], exactly where our current simulation results indicate that the in-plane mechanical stresses are greatest throughout the thickness of the colorectal wall. In addition, residual stretches/stresses significantly affect the magnitudes of stresses in the submucosa during colorectal distension. These insights in combination suggest that changes in residual stretches/stresses under pathophysiological conditions likely contribute to altered visceral mechanotransduction and nociception. We suggest future studies to establish the causal link between residual stretches/stresses and visceral hypersensitivity in symptoms like irritable bowel syndrome.

4.3 Limitations and Outlook. We acknowledge several limitations of our study. We modeled the colorectum as a two-layered, hyperelastic (cylindrical) composite, where each layer assumes homogeneous mechanical properties. In reality, the colorectum contains at least five distinct (if not load-bearing) layers, each of which is likely heterogeneous both radially and axially. Additionally, the colorectum may present time-dependent, viscoelastic behaviors, e.g., Karimi et al. [43]. We also simplified the morphology of the networked fibers in each layer, and the model could be further refined by including additional micromechanical

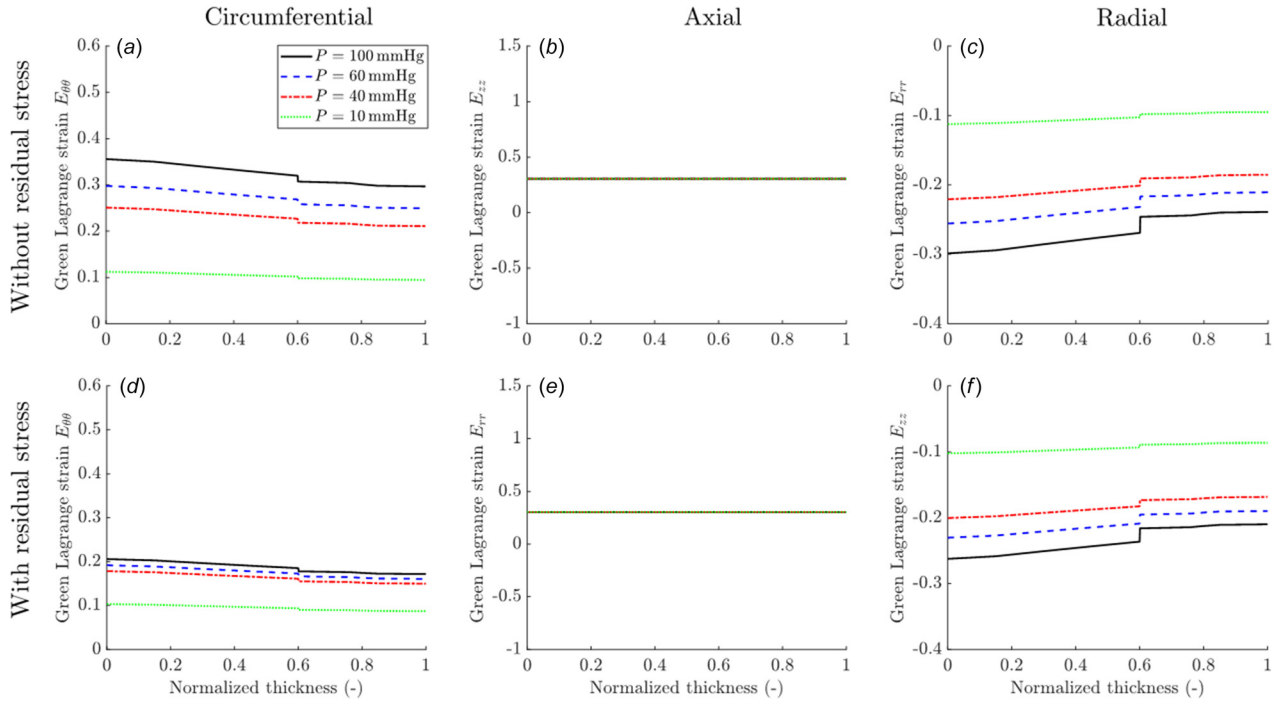

Fig. 9 Plots of the (*a*) and (*d*) circumferential, (*b*) and (*e*) axial, and (*c*) and (*f*) radial (principal) Green–Lagrange strains through the normalized thickness of the rectal segment of the colorectum at $P = 10, 40, 60, 100$ mmHg both (*a–c*) without and (*d–f*) with considering residual stresses

data acquired via imaging, e.g., confocal microscopy with second harmonic generation.

Overall, our results showed the profound impact of residual stresses on the magnitudes and distributions of local mechanical stresses and strains through the wall thickness of the colorectum. Neglecting residual stresses lead to marked over estimations of circumferential stresses, particular at the interface between the inner and outer composite layers. Our simulation results further confirmed our prior experimental observations that the submucosa is the load-bearing structure of the colorectum. Hence, afferent nerve endings strategically located within the submucosa are likely nociceptors that detect concentrations of mechanical stresses to evoke the perception of pain from the viscera. Our models and modeling approaches allow researchers to predict both organ and intratissue biomechanics in the colorectum, and may facilitate better understanding of the underlying mechanical mechanisms of visceral pain and thus aid in establishing treatment targets.

Funding Data

- Division of Civil, Mechanical and Manufacturing Innovation, NSF (Grant No. 1727185; Funder ID: 10.13039/100000147).
- National Institute of Diabetes and Digestive and Kidney Diseases, NIH (Grant No. 1R01DK120824-01; Funder ID: 10.13039/100000062).

Conflicts of Interest

We have no conflicts of interest to report.

References

[1] Siri, S., Zhao, Y., Maier, F., Pierce, D. M., and Feng, B., 2020, "The Macro- and Micro-Mechanics of the Colon and Rectum I: Experimental Evidence," Bioengineering, **7**(4), p. 130.

[2] Zhao, Y., Siri, S., Feng, B., and Pierce, D. M., 2020, "The Macro- and Micro-Mechanics of the Colon and Rectum II: Theoretical and Computational Methods," Bioengineering, **7**(4), p. 152.

[3] Feng, B., and Gebhart, G., 2011, "Characterization of Silent Afferents in the Pelvic and Splanchnic Innervations of the Mouse Colorectum," Am. J. Physiol. Gastrointest. Liver Physiol., **300**(1), pp. G170–G180.

[4] Feng, B., Ho La, J., Schwartz, E. S., and Gebhart, G. F., 2012, "Irritable Bowel Syndrome: Methods, Mechanisms, and Pathophysiology. Neural and Neuro-Immune Mechanisms of Visceral Hypersensitivity in Irritable Bowel Syndrome," Am. J. Physiol. Gastrointest. Liver Physiol., **302**(10), pp. G1085–G1098.

[5] Feng, B., Kiyatkin, M. E., La, J.-H., Ge, P., Solinga, R., Silos-Santiago, I., and Gebhart, G. F., 2013, "Activation of Guanylate Cyclase-c Attenuates Stretch Responses and Sensitization of Mouse Colorectal Afferents," J. Neurosci., **33**(23), pp. 9831–9839.

[6] Moloney, R. D., Johnson, A. C., O'Mahony, S. M., Dinan, T. G., Greenwood-Van Meerveld, B., and Cryan, J. F.,. 2016, "Stress and the Microbiota–Gut–Brain Axis in Visceral Pain: Relevance to Irritable Bowel Syndrome," CNS. Neurosci. Ther., **22**(2), pp. 102–117.

[7] Chen, L., Ilham, S. J., and Feng, B., 2017, "Pharmacological Approach for Managing Pain in Irritable Bowel Syndrome: A Review Article," Anesth. Pain. Med., **7**(2), p. e42747.

[8] Feng, B., and Guo, T., 2020, "Visceral Pain From Colon and Rectum: The Mechanotransduction and Biomechanics," J. Neural Transm., **127**, pp. 415–429.

[9] Clarke, G., Quigley, E. M. M., Cryan, J. F., and Dinan, T. G., 2009, "Irritable Bowel Syndrome: Towards Biomarker Identification," Trends Mol. Med., **15**(10), pp. 478–489.

[10] Camilleri, M., Halawi, H., and Oduyebo, I., 2017, "Biomarkers as a Diagnostic Tool for Irritable Bowel Syndrome: Where Are we?," Expert Rev. Gastroenterol. Hepatol., **11**(4), pp. 303–316.

[11] Spencer, N. J., Kyloh, M., and Duffield, M., 2014, "Identification of Different Types of Spinal Afferent Nerve Endings That Encode Noxious and Innocuous Stimuli in the Large Intestine Using a Novel Anterograde Tracing Technique," PLoS One, **9**(11), p. e112466.

[12] Guo, T., Patel, S. P., Shah, D., Chi, L., Emadi, S., Pierce, D. M., Han, M., Brumovsky, P. R., and Feng, B., 2021, "Optical Clearing Reveals Tnbs-Induced Morphological Changes of vglut2-Positive Nerve Fibers in Mouse Colorectum," Am. J. Physiol. Gastrointest. Liver Physiol., **320**(4), pp. G644–G657.

[13] Siri, S., Maier, F., Chen, L., Santos, S., Pierce, D. M., and Feng, B., 2019, "Differential Biomechanical Properties of Mouse Distal Colon and Rectum Innervated by the Splanchnic and Pelvic Afferents," Am. J. Physiol. Gastrointest. Liver Physiol., **316**(4), pp. G473–G481.

[14] Siri, S., Maier, F., Santos, S., Pierce, D. M., and Feng, B., 2019, "Load-Bearing Function of the Colorectal Submucosa and Its Relevance to Visceral Nociception Elicited by Mechanical Stretch," Am. J. Physiol. Gastrointest. Liver Physiol., **317**(3), pp. G349–G358.

[15] Maier, F., Siri, S., Santos, S., Chen, L., Feng, B., and Pierce, D. M., 2021, "The Heterogeneous Morphology of Networked Collagen in Distal Colon and Rectum of Mice Quantified Via Nonlinear Microscopy," J. Mech. Beh. Biomed. Mat., **113**, p. 104116.

[16] Alastrué, V., Peña, E., Martínez, M. Á., and Doblaré, M., 2007, "Assessing the Use of the "Opening Angle Method" to Enforce Residual Stresses in Patient-Specific Arteries," Ann. Biomed. Eng., **35**(10), pp. 1821–1837.

[17] Zhao, J., Chen, X., Yang, J., Liao, D., and Gregersen, H., 2007, "Opening Angle and Residual Strain in a Three-Layered Model of Pig Oesophagus," J. Biomech., **40**(14), pp. 3187–3192.

[18] Ciarletta, P., Destrade, M., and Gower, A. L., 2016, "On Residual Stresses and Homeostasis: An Elastic Theory of Functional Adaptation in Living Matter," Sci. Rep., **6**, p. 24390.

[19] Fung, Y. C., 1983, "On the Foundations of Biomechanics," ASME J. Appl. Mech., **50**(4b), pp. 1003–1009.

[20] Vaishnav, R. N., and Vossoughi, J., 1983, "Estimation of Residual Strains in Aortic Segments," *Biomedical Engineering II: Recent Developments*, C. W. Hall, ed., Pergamon Press, New York, pp. 330–333.

[21] Chuong, C. J., and Fung, Y. C., 1983, "Three-Dimensional Stress Distribution in Arteries," ASME J. Biomech. Eng., **105**(3), pp. 268–274.

[22] Chuong, C. J., and Fung, Y. C., 1986, "On Residual Stress in Arteries," ASME J. Biomech. Eng., **108**(2), pp. 189–192.

[23] Fung, Y. C., 1991, "What Are the Residual Stresses Doing in Our Blood Vessels?," Ann. Biomed. Eng., **19**(3), pp. 237–249.

[24] Vaishnav, R. N., and Vossoughi, J., 1987, "Residual Stress and Strain in Aortic Segments," J. Biomech., **20**(3), pp. 235–239.

[25] Matsumoto, T., and Hayashi, K., 1996, "Stress and Strain Distribution in Hypertensive and Normotensive Rat Aorta Considering Residual Strain," ASME J. Biomech., **118**(1), pp. 62–73.

[26] Delfino, A., Stergiopulos, N., Moore, J. E., Jr., and Meister, J.-J., 1997, "Residual Strain Effects on the Stress Field in a Thick Wall Finite Element Model of the Human Carotid Bifurcation," J. Biomech., **30**(8), pp. 777–786.

[27] Holzapfel, G. A., Gasser, T. C., and Ogden, R. W., 2000, "A New Constitutive Framework for Arterial Wall Mechanics and a Comparative Study of Material Models," J. Elasticity, **61**(1/3), pp. 1–48.

[28] Peterson, S. J., and Okamoto, R. J., 2000, "Effect of Residual Stress and Heterogeneity on Circumferential Stress in the Arterial Wall," ASME J. Biomech. Eng., **122**(4), pp. 454–456.

[29] Raghavan, M. L., Trivedi, S., Nagaraj, A., McPherson, D. D., and Chandran, K. B., 2004, "Three-Dimensional Finite Element Analysis of Residual Stress in Arteries," Ann. Biomed. Eng., **32**(2), pp. 257–263.

[30] Holzapfel, G. A., and Ogden, R. W., 2010, "Modelling the Layer-Specific 3D Residual Stresses in Arteries, With an Application to the Human Aorta," J. R. Soc. Interface, **7**(46), pp. 787–799.

[31] Pierce, D. M., Fastl, T. E., Rodriguez-Vila, B., Verbrugghe, P., Fourneau, I., Maleux, G., Herijgers, P., Gomez, E. J., and Holzapfel, G. A., 2015, "A Method for Incorporating Residual Stretches/Stresses Into Patient-Specific Simulations of Arteries," J. Mech. Beh. Biomed. Mat., **47**, pp. 147–164.

[32] Zhao, Y., Siri, S., Feng, B., and Pierce, D. M., 2021, "Computational Modeling of Mouse Colorectum Capturing Longitudinal and Through-Thickness Biomechanical Heterogeneity," J. Mech. Beh. Biomed. Mat., **113**, p. 104127.

[33] Feng, B., La, J. H., Schwartz, E. S., Tanaka, T., McMurray, T. P., and Gebhart, G. F., 2012, "Long-Term Sensitization of Mechanosensitive and -Insensitive Afferents in Mice With Persistent Colorectal Hypersensitivity," Am. J. Physiol. Gastrointest. Liver Physiol., **302**(7), pp. G676–G683.

[34] Holzapfel, G. A., Unterberger, M. J., and Ogden, R. W., 2014, "An Affine Continuum Mechanical Model for Cross-Linked F-Actin Networks With Compliant Linker Proteins," J. Mech. Beh. Biomed. Mat., **38**, pp. 78–90.

[35] Pierce, D. M., Unterberger, M. J., Trobin, W., Ricken, T., and Holzapfel, G. A., 2016, "A Microstructurally Based Continuum Model of Cartilage Viscoelasticity and Permeability Incorporating Measured Statistical Fiber Orientations," Biomech. Model. Mechanobiol., **15**(1), pp. 229–244.

[36] Maas, S. A., Ellis, B. J., Ateshian, G. A., and Weiss, J. A., 2012, "FEBio: Finite Elements for Biomechanics," ASME J. Biomech. Eng., **134**(1), p. 011005.

[37] Maas, S. A., Erdemir, A., Halloran, J. P., and Weiss, J. A., 2016, "A General Framework for Application of Prestrain to Computational Models of Biological Materials," J. Mech. Beh. Biomed. Mat., **61**, pp. 499–510.

[38] Feng, B., Brumovsky, P. R., and Gebhart, G. F., 2010, "Differential Roles of Stretch-Sensitive Pelvic Nerve Afferents Innervating Mouse Distal Colon and Rectum," Am. J. Physiol. Gastrointest. Liver Physiol., **298**(3), pp. G402–G409.

[39] Feng, B., and Guo, T., 2020, "Visceral Pain From Colon and Rectum: The Mechanotransduction and Biomechanics," J. Neural. Transm., **127**(4), pp. 415–429.

[40] Gregersen, H., Kassab, G. S., and Fung, Y. C., 2000, "The Zero-Stress State of the Gastrointestinal Tract: Biomechanical and Functional Implications," Dig. Dis. Sci., **45**(12), pp. 2271–2281.

[41] Du, Y., Lü, C., Liu, C., Han, Z., Li, J., Chen, W., Qu, S., and Destrade, M., 2019, "Prescribing Patterns in Growing Tubular Soft Matter by Initial Residual Stress," Soft Matter, **15**(42), pp. 8468–8474.

[42] Sigaeva, T., Sommer, G., Holzapfel, G. A., and Di Martino, E. S., 2019, "Anisotropic Residual Stresses in Arteries," J. R. Soc. Interface, **16**(151), p. 20190029.

[43] Karimi, A., Shojaei, A., and Razaghi, R., 2017, "Viscoelastic Mechanical Measurement of the Healthy and Atherosclerotic Human Coronary Arteries Using Dic Technique," Artery Res., **18**(C), pp. 14–21.